Journal of Materials Chemistry C

Polarized Resonance Synchronous Spectroscopy as a Powerful Tool for Studying the Kinetics and Optical Properties of Aggregation-Induced Emission

Journal:	*Journal of Materials Chemistry C*
Manuscript ID	TC-ART-07-2019-004106.R1
Article Type:	Paper
Date Submitted by the Author:	22-Aug-2019
Complete List of Authors:	Xu, Joanna; Mississippi State University Department of Chemistry, Niu, Guangle; Hong Kong University of Science and Technology, Tang, Ben Zhong; The Hong Kong University of Science and Technology, Department of Chemistry Zhang, Dongmao; Mississippi State University, Chemistry

Polarized Resonance Synchronous Spectroscopy as a Powerful Tool for Studying the Kinetics and Optical Properties of Aggregation-Induced Emission

Joanna Xiuzhu Xu, [⊥] *Guangle Niu,* [△] *Ben Zhong Tang,* [△] *and Dongmao Zhang*[*,⊥]

[⊥] Department of Chemistry, Mississippi State University, Mississippi State, Mississippi, 39762, United States

[△] Department of Chemistry, The Hong Kong University of Science and Technology, Clear Water Bay, Kowloon, 999077, Hong Kong, China

[*] Corresponding authors: Dongmao@chemistry.msstate.edu

ABSTRACT

Light scattering and absorption both contribute to the UV-vis extinction quantified with UV-vis spectrophotometer, but they differ drastically in their causes and effects. Existing optical studies have been generally focused on the fluorescence and total photon extinction of the aggregation-induced-emission (AIE) materials. The effects of aggregation on the light absorption and scattering of AIE luminogen (AIEgen) are essentially unexplored. Herein, we reported a spectroscopic study of the structures and properties of AIE aggregates using the combination of UV-vis, fluorescence, and the polarized resonance synchronous spectroscopy (PRS2) methods. Optical activities including the light absorption extinction, scattering extinction, and absorbance-normalized fluorescence emission have been quantified for the first time for the AIE aggregates prepared with an in-house prepared AIEgen 2-((4-(Diphenylamino) biphenyl-4-yl) methylene) malononitrile (TPMN). Absorption extinction dominates the entire UV-vis extinction spectrum obtained with the dissolved TPMN. For the UV-vis spectrum acquired with TPMN aggregates, however, scattering extinction accounts for up to 35% of the peak photon extinction at 480 nm. This number rises to 100% in the wavelength region beyond 580 nm. Sample incubation increases the light scattering extinction, scattering depolarization, and fluorescence emission of the TPMN aggregate, but reduces its light absorption extinction. With its ability to provide information inaccessible with existing techniques, this work demonstrates that PRS2 is powerful tool for AIE materials in quantifying their optical properties and monitoring the aggregation/disaggregation processes.

INTRODUCTION

Aggregation-induced-emission (AIE) has become an increasingly active area of research. Generally, AIE luminogens (AIEgens) have no or low luminescent activities in their isolated forms, but become strongly luminescent in their aggregated forms. The aggregation-enhanced emission is in sharp contrast to what has been generally observed in traditional fluorophores for which aggregation usually quenches the fluorescence emission. Since the term AIE was coined in 2001,[1] the number of AIE-related publication has grew exponentially in the area of organic optoelectrical devices,[2,3] chemical and biological sensors,[4,5] cell imaging,[6-8] multi-responsive materials[9,10] and polymer sciences[11].

In contrast to the rich information on AIE fluorescence, mechanistic understanding of the origins of the UV-vis extinction spectral change induced by AIEgen aggregation has been limited. Existing literatures commonly interpret the UV-vis spectra of AIE aggregates as their UV-vis absorbance spectra without considering the contribution of light scattering extinction. This practice can be highly problematic considering that scattering cross-section is usually proportional to the sixth power of the scatterers' radius.[12] The size of an AIE aggregates usually spans from 50 nm to 200 nm in radius.[13,14] As a result, the scattering cross-section of an AIE aggregate can be up to 12 orders of magnitude higher than that of individual AIEgen molecules. Such high scattering cross-section explains why most of the literature AIE samples are visually turbid.

Light scattering and absorption both contribute to the UV-vis extinction quantified with the UV-vis spectrophotometers. However, they differ drastically in their causes and effects. Therefore, quantitative determination of the light scattering and absorption activities of the AIE materials is important for their design and applications. For examples, it is the absorbed photons,

but not the scattered ones, responsible for the AIE-based singlet oxygen in photodynamic therapy and the fluorescence emission in biomedical imaging. Furthermore, light scattering and absorption reveals different information of the analytes. While light scattering extinction intensity is directly related to the scatterers' particle size and chemical compositions, the scattering depolarization spectrum provides rich information on the scatterer's geometry.[15,16] Earlier works demonstrated the scattering depolarization of spherical solvent molecules and gold nanoparticles is very close to zero crossing the entire UV-vis region, while their rod-shaped counterparts all possess relatively high peak scattering depolarization.[15,17]

Quantitative decomposition of the UV-vis extinction spectra of the AIE aggregates into their scattering and absorption extinction component spectra is critical also for reliable determination of their fluorescence properties. Since AIE experiments are usually performed with relatively concentrated samples (10 μM or above) where the photon extinction is usually high, one should consider the potential sample inner-filter-effect (IFE) on the measured fluorescence intensity for the AIE aggregates, [18] and the multiplicative light scattering effect in determination of the AIE fluorescence depolarization/anisotropy. [19] However, only photon absorption extinction, but not scattering extinction, induces significant sample IFE.[18] Conversely, only scattering extinction, but no absorption extinction, enhances the fluorophore fluorescence depolarization.[19] Therefore, UV-vis extinction spectral decomposition is a prerequisite for reliable quantification of the fluorescence intensity and anisotropy for the AIE aggregates.

In theory, one can avoid the complication of sample light absorption and scattering on fluorescence measurements by using diluted samples with photon extinction less than 0.05.[20] However, this approach is generally inapplicable to AIE samples for the following reasons. First, by definition, all AIE study must be performed with an AIEgen concentration surpasses its

saturation solubility, which can be a few micromolars even in the poor AIEgen solvent.[1,21-23] Second, even when AIEgen can aggregate at a low- or sub-micromolar concentration, the concentration of AIE aggregates responsible for the fluorescence signal may be too low for reliable fluorescence acquisition. For example, it takes approximately one million AIEgen molecules with a molecular diameter of 2 nm to form one AIE aggregate with a diameter of 200 nm. In this case, the concentration of the AIE aggregates, the actual fluorescence emitters, is only 10 pM when precursor AIEgen concentration is as high as 10 μM. Such a low AIE aggregate concentration is unlikely sufficient for reliable fluorescence measurement with conventional spectrofluorometers.

Herein, we quantify the optical properties of these AIE aggregates with the recent polarized resonance synchronous spectroscopic (PRS2) method.[24] When used in combination with UV-vis spectrophotometric and spectrofluorometric measurements, the PRS2 method has enabled the first-time quantitative decoupling of the material photon absorption, scattering, and on-resonance fluorescence (ORF) that can concurrently occur for fluorescence materials under the resonance excitation and detection conditions.[24] The resonance excitation and detection refer to the measurements performed by keeping the excitation and detection wavelength identical during the spectral acquisition. PRS2 spectra are acquired with conventional spectrofluorometer equipped with an excitation linear polarizer and a detection linear polarizer. Mathematically, the fluorophore light scattering spectrum $\sigma_f^{sca}(\lambda)$ and ORF cross-section spectrum $\sigma_f^{ORF}(\lambda)$ can be readily performed with Eq. 1 and Eq. 2, respectively, using polytyrene nanoparticle (PSNP) as an external reference.

$$\sigma_f^{sca}(\lambda) = \frac{(1 + 2P_f^{sca}(\lambda))\ C_{PSNP} I_{f,VV}^{PRS2,sca}(\lambda,W)}{(1 + 2P_{PSNP}^{sca}(\lambda))\ C_f I_{PSNP,VV}^{PRS2,sca}(\lambda,W)} \sigma_{PSNP}^{sca}(\lambda) \qquad (1)$$

$$\sigma_f^{ORF}(\lambda) = \frac{(1 + 2P_f^{ORF}(\lambda))\ \ C_{PSNP} I_{f,VV}^{PRS2,F}(\lambda,W)}{(1 + 2P_{PSNP}^{sca}(\lambda))W\ \ C_f I_{PSNP,VV}^{PRS2,F}(\lambda,W)} \sigma_{PSNP}^{sca}(\lambda) \qquad (2)$$

$\sigma_{PSNP}^{sca}(\lambda)$ is the PSNP scattering cross-section spectrum. Since PSNPs are light scatterers with no signficant photon absorption in the wavelength region from 300 nm to 800 nm, its scattering cross-section spectrum $\sigma_{PSNP}^{sca}(\lambda)$ is determined straightforwardly by using its UV-vis extinction spectrum.[24] $I_{f,VV}^{PRS2,sca}(\lambda,W)$ and $I_{f,VV}^{PRS2,F}(\lambda,W)$ are fluorophore PRS2 fluorescence and light scattering VV spectra, respectively. Procedures for decompositing the sample PRS2 spectra into its fluorescence and light scattering component spectrum is avaiable from a recent publication.[25] $I_{PSNP,VV}^{PRS2,sca}(\lambda,W)$ is the experimental PRS2 VV spectra obtained with PSNP. W is the wavelength bandwidth used for the excitation and detection monochromators. The subscript "VV" indicates that the PRS2 spectra are acquired with vertically polarized excitation (first V) and vertically polarized detection (second V). In this case, both the excitation and detected light are linearly polarized in perpendicular to the instrument plane defined by the excitation lamp, cuvette holder, and detector. $P_f^{sca}(\lambda)$ and $P_f^{ORF}(\lambda)$ are the fluorophore light scattering and ORF depolarization respectively, which are the ratio between their respective PRS2 VH and VV spectra. Detailed description of the equation derivation, spectral acquistion, and data analysis procedures are available in earlier publications.[18,25,26]

EXPERIMENTAL

Chemicals and Instruments. The model AIEgens used in this study is the in-house prepared 2-((4'-(Diphenylamino) biphenyl-4-yl) methylene) malononitrile (TPMN).[27] Acentonitrile are obtained from Sigma Aldrich and they are used as received. Nanopure water is

used throughout the experiment. DLS measurements are performed on an Anton-Paar DLS instrument at 25 ˚C.

Optical spectroscopic measurements and data analysis. The UV-vis extinction spectra were obtained with a OLIS Cary-14 UV/Vis/NIR double beam spectrophotometer. The Stokes'-shifted fluorescence (SSF) and PRS2 spectra were acquired with a Horiba FluoroMax-4 spectrofluorometer equipped with an excitation and a detection linear polarizers. Unless specified otherwise, all the spectrofluorometer-based spectral acquisitions were performed with an intergration time 0.3 s, and a slit width 2 nm for both the excitation and detection monochromators. The S1/R1 spectra are taken in this work, where the signal from sample detector (S1) was normalized by that from the reference detector (R1) to eliminate the flutuations from the Xeon light source. Unless specified otherwise, all data are obtained with TPMN aggregates aged for 48 hours.

The presented PRS2 spectra data are IFE-corrected, and solvent- and cuvette-background subtracted using an established method.[24] The effective excitation and detection pathlengths of the spectrofluorometer used for the IFE-correction were 0.58 cm and 0.60 cm, respectively,[28,29] which were quantified before using a water Raman method.[28] The G-factor spectrum needed to correct the detector polarization bias in PRS2 and polarized fluorescence excitation spectra was quantified eariler.[24]

Sample incubation of TPMN aggregates. A 60 μM aggregated TPMN in water/ACN (*v*/*v*, 90/10) solvent mixture is prepared as follows: 600 μM TPMN is dissolved in ACN as the stock solution, 0.3 mL of which is subsequently mixed with 2.7 mL of water. Time-dependent UV-

vis, PRS2, fluorecence spectra are taken for investigation of the effect of sample incubation on the optical properties of the TPMN aggregates.

Disaggregation of the TPMN aggregates. 80 μM TPMN was aggregated in water/ACN (*v*/*v*, 90/10) solvent mixture and allowed to equilibrate for 48 hours before diluting 4 times with water to make a disaggregation sample of 20 μM in water/ACN (*v*/*v*, 72.5/27.5) solvent mixture. Two control samples are prepared by diluting TPMN in ACN into water/ACN (*v*/*v*, 72.5/27.5) mixture solvent. The second one is diluting the prepared TPMN aggregate in water/ACN (*v*/*v*, 90/10) with the same mixture solvent. The TPMN concentrations in these three samples are the same.

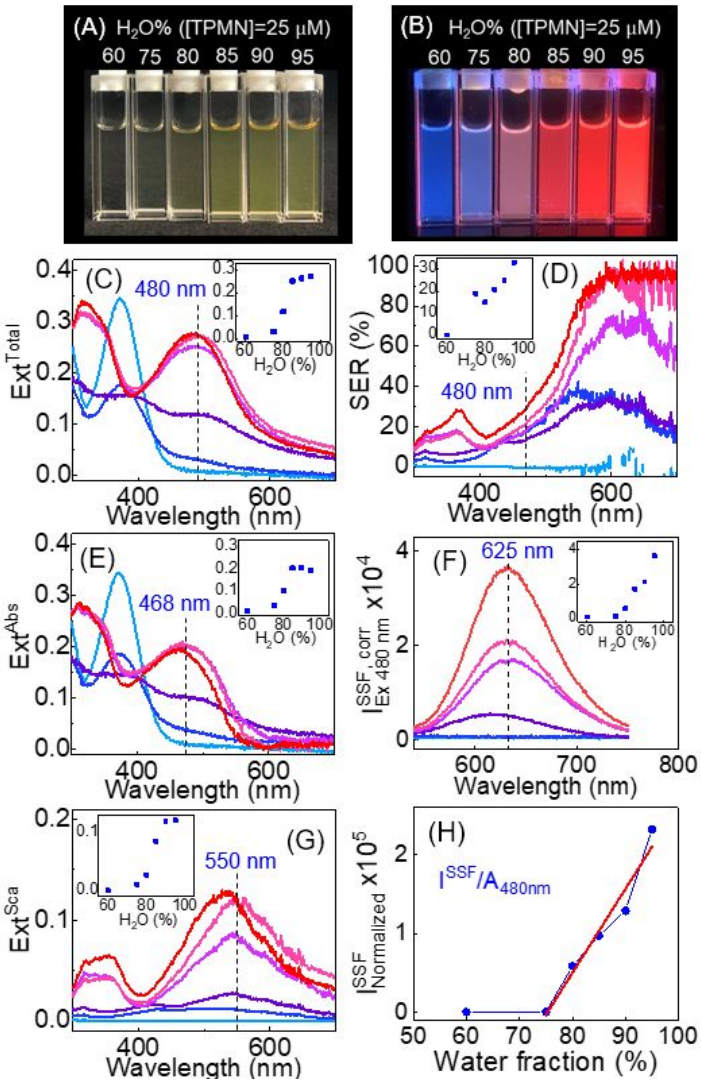

Figure 1. (A) Bright field and (B) fluorescence photograph of the TPMN samples differing only in their solvent water/ACN ratio. The water fraction is shown in the photos. The nominal TPMN concentration is 25 μM for all samples. (C) UV-vis extinction spectra of TPMN aggregates of different water fractions. The color coding from blue to red indicates increasing water fractions. Inset: Peak extinction intensity at 480 nm as a function of the water fraction. (D) The scattering to extinction ratio (SER) spectra. Inset: Percentage scattering contribution to the total extinction at the peak extinction wavelength at 480 nm. (E) Absorption extinction spectrum. Inset: Peak absorption extinction at 468 nm as a function of water fraction. (F) IFE-corrected stokes-shifted fluorescence (SSF) spectrum excited at 480 nm. Inset: Peak fluorescence intensity at 625 nm as a function of the water fraction. (G) Scattering extinction spectra. Inset: Peak scattering extinction intensity at 550 nm as a function of the water fraction. (H) the absorbance-normalized IFE-corrected peak fluorescence intensity as a function of the water concentration. All measurements are performed after 48-hour incubation and completed within half an hour. The experimental PRS2 spectra and as-acquired fluorescence spectra were presented in Figure S1 and S2, Supporting Information.

RESULTS AND DISCUSSIONS

Optical activities of AIEgen aggregates. TPMN with a nominal concentration of 25 μM is soluble in the ACN/water mixture with a water fraction up to 60% (Figure 1A and 1B). Dissolved TPMN has no detectable fluorescence activities. The blue color in the samples containing 60% and 75% water are the background from the UV illuminator (Figure 1B). Significant fluorescence (Figure 1D) appears only when the TPMN aggregates are visually appreciable (Figure 1A and 1B).

Similar to what observed with TPMN (Figure 1C), aggregation often induces significant change in AIEgen UV-vis extinction spectrum, the sum of AIEgen UV-vis absorption extinction and scattering extinction. There is to our knowledge, however, no prior work on quantifying the effect of AIEgen aggregation on its absorption and scattering activities. Apparently, the UV-vis spectra of the aggregated TPMN differ drastically from that dissolved in ACN and in ACN/water mixture solvents with low water fractions (Figure 1C), so are the TPMN Stokes-shifted fluorescence (SSF) spectrum (Figure 1F). However, the UV-vis and fluorescence spectra of the TPMN aggregates are remarkably different in their water fraction dependence. The UV-vis extinction spectra of the three highest water fraction samples are approximately the same (Figure 1C), while the fluorescence intensity monotonically increases with the increasing water fraction (Figure 1D). The fluorescence intensity for the 95% water fraction sample is approximately two times higher than that for sample with 85% water fraction (Figure 1F). This observation leads to an intriguing question why the fluorescence intensity can be so different among the TPMN aggregates that have nearly identical UV-vis extinction spectra. Mechanistically, this phenomenon can be due to enhanced fluorescence quantum yield, enhanced photon absorption, or both for the TPMN aggregates in higher water fractions.

To answer this problem, one needs decompose the TPMN UV-vis extinction spectra into its absorption (Figure 1E) and scattering (Figure 1G) extinction component spectra. Such spectral decomposition was performed using the PRS2 method described before.[25] Since the absorbance of the aggregated TPMN prepared with the three highest water fractions are essentially the same (Figure 1E), the fluorescence intensity difference among these samples must be due to the difference in their fluorescence quantum yield, i.e, the AIE aggregates prepared with a higher water fraction have higher fluorescence quantum yields (Figure 1H).

While absorption extinction dominates the UV-vis extinction spectra for the dissolved TPMN, scattering becomes an important contributor to UV-vis extinction of the aggregated TPMN. Furthermore, the scattering extinction contribution to the UV-vis spectra of the TPMN aggregates is strongly wavelength dependent. As an example, ~35.0% of UV-vis extinction for the 95% water fraction sample at its peak UV-vis wavelength at 480 nm is due to the TPMN scattering extinction (Figure 1D), while the UV-vis extinction for this sample in the wavelength region beyond 580 nm is due entirely to the light scattering.

Unlike the PSNP and nonabsorbing small molecule solvents including water and dichloromethane that are nearly perfect Rayleigh scatterers with light scattering extinction proportional to the inverse fourth power of the excitation wavelength,[17] the scattering extinction spectra of TPMN aggregates are quite complicated in their excitation wavelength dependence. Furthermore, the UV-vis total extinction, absorption extinction, and scattering extinction peak wavelengths for the aggregated TPMN are all different. The peak UV-vis extinction, absorption extinction, and scattering extinction wavelengths are ~480 nm, ~468 nm, and 550 nm, respectively for the three most-fluorescence-active samples. Mechanistic understanding of the UV-vis absorption and scattering extinction features are currently impossible because they require detailed

information about the size and shape distribution of the aggregated TPMN and the intermolecular interactions among TPMN molecules in the aggregates. The data in Figure 1 highlights the complicity of the photo absorption, scattering, and emission of the AIE aggregates

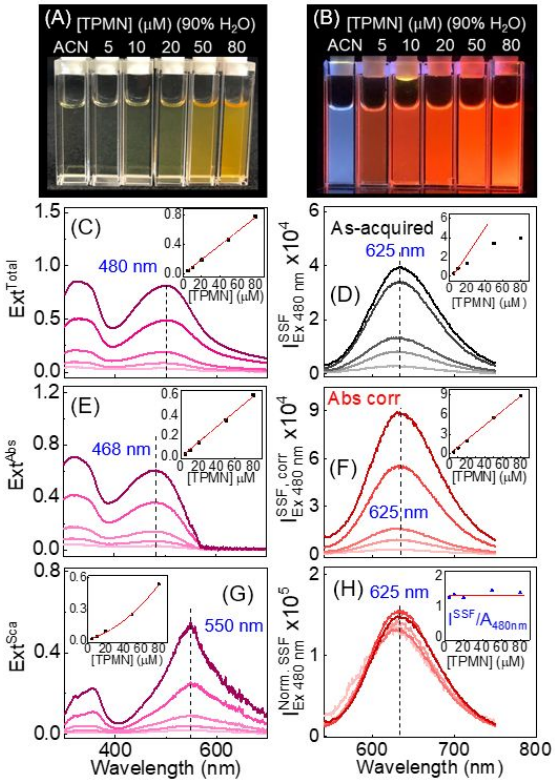

Figure 2: (A) Bright-field and (B) Fluorescence photographs of TPMN in (first cuvette) pure ACN and (last five cuvettes) ACN/Water (*v*/*v*, 10:90) mixture solvent. The TPMN concentration in ACN is 10 μM while that in the ACN/water mixture solvent is 5 μM, 10 μM, 20 μM, 50 μM and 80 μM, respectively. (C) UV-vis extinction spectra as a function of the TPMN concentration in ACN/water mixture solvent. Inset: The peak UV-vis intensity as a function of the TPMN concentration. (D) as-acquired fluorescence intensity as a function of the TPMN concentration in ACN/water mixture solvent. Inset: The peak fluorescence intensity as a function of the TMPN concentration. (E) UV-vis absorption extinction spectra as a function of the TPMN concentration in ACN/water mixture solvent. Inset: the peak UV-vis absorption intensity as a function of the TPMN concentration. (F) The IFE-corrected fluorescence spectra where only the sample photon absorbance is used for the IFE correction. Inset: Peak IFE-corrected fluorescence intensity as a function of the TPMN concentration. (G) UV-vis scattering extinction spectra as a function of the TPMN concentration in ACN/water mixture solvent. Inset: The peak UV-vis scattering intensity as a function of the TPMN concentration. (H) Absorbance-normalized IFE-corrected fluorescence spectra as a function of the TPMN concentration in ACN/water mixture.

None of the TPMN aggregates exhibited detectable on-resonance-fluorescence (ORF) when excited in the wavelength region where the TPMN UV-vis absorbance spectrum and fluorescence spectrum overlaps (Figure S2, Supporting information). This observation is in sharp contrast to common molecular fluorophores such as rhodamine dyes for which ORF appears when excited in the wavelength region where the fluorophore both absorbs and emits.[17] One possible reason is the TPMN ORF quantum yield is too low. Nonetheless, the lack of TPMN ORF enables us to treat the aggregated TPMN as a simultaneous photon absorber and scatterer but not emitter under the resonance excitation and detection condition. In this case, the IFE-corrected and solvent-background-subtracted PRS2 spectra are the polarized light scattering intensity spectra needed for calculating the light scattering extinction.[26]

The successful separation of the TPMN light scattering and absorption contribution to its UV-vis extinction paves the way for quantification of the TPMN fluorescence activity as a function of the TPMN concentration. The amount of aggregate increases with increasing TPMN concentrations (Figure 2A), so is the brightness of these samples (Figure 2B). Such a visual observation is consistent with the UV-vis extinction and fluorescence spectral measurements. Both UV-vis (Figure 2C) and fluorescence intensity (Figure 2D) monotonically increases with increasing TPMN concentrations.

The peak UV-vis extinction and absorption intensities of the TPMN aggregates are approximately linearly dependent on the TPMN concentrations (Figure 2C and 2E), but the as-acquired peak fluorescence intensities increase nonlinearly with the TPMN concentrations (Figure 2D). Such nonlinearity can be due to the sample inner filter effect (IFE) induced by the sample photon absorption at the excitation and detection wavelength, and/or from the intrinsic difference in optical property of the TPMN aggregates prepared with different TPMN concentrations. The

nearly perfect linearity between the IFE-corrected fluorescence intensity (Figure 2F) as a function of the TPMN concentration indicates that the fluorescence activities of the aggregated TPMN are the same (Figure 2H).

The peak scattering extinction is increasing quadratically on the TPMN precursor concentration (Figure 2G), which is in sharp contrast to the peak UV-vis extinction, absorbance, and IFE-corrected fluorescence intensities of the aggregated TPMN that are all approximately linearly dependent on the TMPN precursor concentrations. Using UV-vis absorption extinction, scattering extinction, and fluorescence emission intensity shown in Figure 2, one can estimate the absolute light scattering and absorption cross-sections (Figure S3, Supporting information), and the relative fluorescence quantum yields for the aggregated TPMN molecules, the absorbance-normalized IFE-corrected TPMN fluorescence intensity (Figure 2H). These calculations are performed by assuming all TPMN molecules are aggregated in the 90% water solvent. The peak absorption and extinction cross-sections at 480 nm (Figure S3, Supporting information) and relative fluorescence quantum yields (Figure 2H) for the TPMN molecules are constant regardless of the TPMN concentration used for the aggregate formation, while the peak light scattering cross-section at 550 nm increases linearly with the TPMN precursor concentration (Figure S3, Supporting information).

The light scattering cross-section data strongly indicates that the average size of the TPMN aggregates increases with increased TPMN precursor concentration. Assuming TPMN aggregates to be Rayleigh scatterers, their light scattering cross-sections are proportional to the square of the scatterer's volume ($\sigma^{Sca} \propto V^2$). In contrast, the constant absorption cross-section and fluorescence quantum yield of the TPMN aggregates prepared with different precursor concentration indicates

the photon absorption and emission activity of the aggregated TPMN molecules are essentially the same regardless of the size distribution of the aggregates.

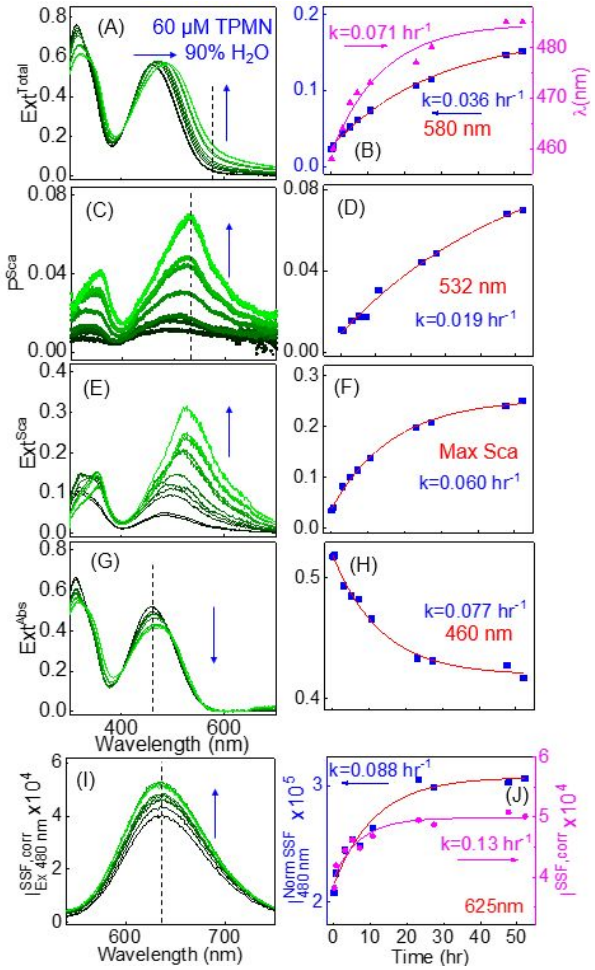

Figure 3. Effect of sample incubation on the optical properties of the TPMN aggregates prepared with 60 μM TPMN in (*v:v*) 10:90 H_2O/ACN mixture. (A) Extinction intensity spectra. (B) Blue dots are the extinction intensities at the wavelength indicated by the dash line in (A) while the pink dots are the peak extinction wavelength of TPMN as a function of the sample incubation time. (C) Scattering depolarization spectra. (D) Scattering depolarization at wavelength highlighted in (C) as a function of the incubation time, (E) Scattering extinction spectra. (F) the time course of the scattering extinction at wavelength highlighted in (E). (G) absorption extinction spectra, (H) the time-course of the absorption extinction at the wavelength indicated in (G). (I) IFE-corrected SSF spectra, (J) (blue dots) the time course of the absorbance-normalized IFE-corrected SSF intensities and (pink dots) IFE-corrected SSF intensities. The solid lines in (B, D, F, H, and J) are the empirical curve-fitting for the data in pink with $y = y_0 e^{(-kt)}$ and for the data in blue with $y = y_0 (1 - e^{(-kt)})$. The values of k are rate constants from the empirical fitting. The as-acquired data are presented in Figure S4, Supporting Information.

Effects of the sample incubation. Sample incubation has a significant effect on the optical properties of the TPMN aggregates in terms of their photon absorption extinction, scattering extinction, and fluorescence emission. Before reaching their respective constant values after approximately two-and-half days of sample incubation of TPMN aggregates prepared with 60 μM TPMN in (*v:v*) 10:90 ACN/H_2O mixture, the peak wavelengths of UV-vis total extinction (Figure 3A), scattering extinction (Figure 3E), and absorption extinction (Figure 3G) all monotonically red-shift with increasing sample incubation time. However, the effect of the sample incubation on their peak intensities are very different. Sample incubation introduces no significant changes in the TPMN peak extinction intensity in the 480 nm region (Figure 3A), but reduces its absorption extinction (Figure 3G) and increases its scattering extinction (Figure 3E). Most strikingly, despite of the decreased sample photon absorption as a function of the sample incubation (Figure 3G and 3H), the SSF intensity increases as the sample ages (Figure 3I and 3J). The time-course of the absorbance-normalized SSF (blue curve in Figure 3J) indicates that the sample incubation enhances the fluorescence quantum yield of the TPMN aggregates.

The changes in the explored optical properties (Figure 3) are indicative of internal structure change in the TPMN aggregates as a function of incubation time. If sample incubation only changes the size of the TPMN aggregates but not their internal structures, one should expect the only the change in the TPMN light scattering cross-section (Figure 3E and 3D) and scattering depolarization (Figure 3C and 3D), but not in UV-vis absorption extinction and TPMN fluorescence activities.

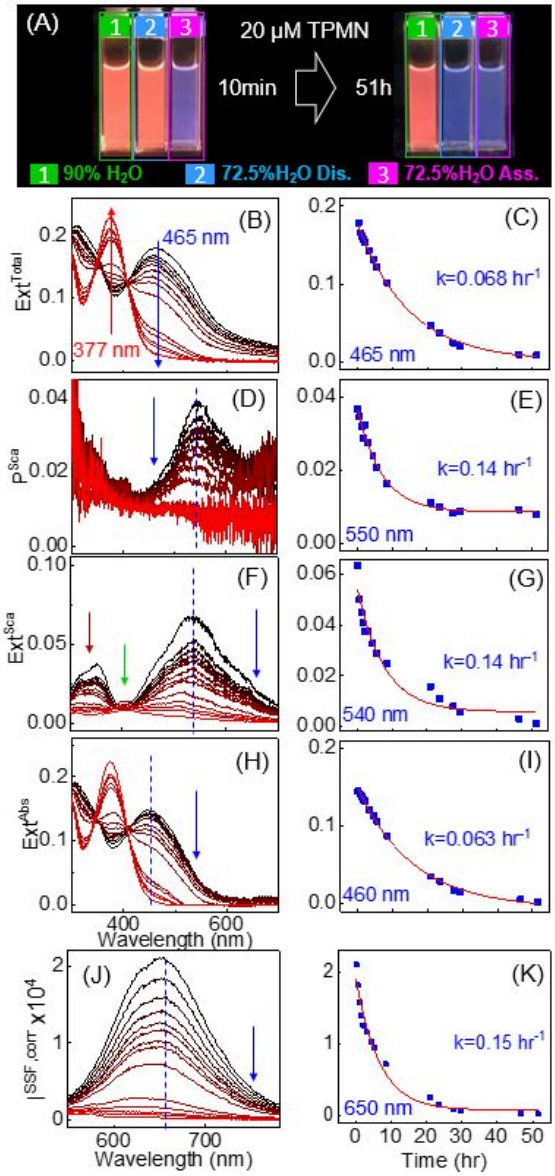

Figure 4. (A) Fluorescence photographs of 20 μM TPMN in (cuvette 1) 90% H_2O, (cuvette 2) first aggregated in 90% H_2O then disassembled upon dilution with ACN into 72.5% H_2O (72.5% H_2O Dis.), (cuvette 3) first in 100% ACN then assembled upon dilution with water into 72.5% H_2O (72.5% H_2O Ass.). The data shown in Figure (B-K) are all acquired for the sample in cuvette 2. (B) Extinction spectra, (C) the time-course of the extinction intensity of the sample at the wavelength of 465 nm. (D) scattering depolarization spectra. (E) the time course of the light scattering depolarization. (F) scattering extinction spectra, (G) the time course of sample scattering extinction. (H) absorption extinction spectra, (I) the time-course of the absorption extinction at the wavelength indicated in (H). (J) IFE-corrected SSF spectra, (K) the time-course of the IFE corrected fluorescence intensity at wavelength indicted in (J). The solid lines and the k values in (C, E, G, I, K) were obtained by empirical curve-fitting of the experimental data as a first order process ($y = y_0 e^{(-kt)}$). The as-acquired SSF, analyte-specific PRS2 spectra, DLS analysis are in Figure S5, Supporting Information.

Effects of AIEgen disaggregation. Existing AIE research has almost focused exclusively on AIEgen aggregation. Insights to the processes and optical properties of the disaggregation of the aggregated AIE materials is critical for developing a comprehensive understanding of formation mechanism of the AIE aggregations and applications where the sample matrix may change. TPMN aggregation is an entirely reversible process, and its aggregation and disaggregation are both rapid. The onset of the TPMN aggregation is instantaneous upon addition of sufficient water into TPMN in ACN solution, and it takes only about 50 hours for the aggregated TPMN to reach its approximately constant photon absorption, scattering, and fluorescence emission activities (Figure 3). Conversely, the onset of aggregate disintegration is also instantaneous upon addition of good solvent ACN into the TPMN aggregates in 90% water (Figure 4) to reduce the water fraction down to 72%. Disaggregation also completed approximately within 50 hours of the good solvent addition.

Compare and contrast the aggregation and disaggregation kinetics of TPMN with the respective counterparts for *meso*-tetrakis (4-sulfonatophenyl) porphyrin (TSPP) is revealing about the intermolecular interactions within aggregated TPMN. The rapid solvent-induced TPMN aggregation is in sharp contrast to the slow kinetics reported for pH-induced TSPP aggregation.[30] TSPP exists as dissolved molecules in basic solutions, but aggregates in strongly acidic solutions. However, both TSPP aggregation and disaggregation are an extraordinarily lengthy process. It took more than 127 days for the aggregated TSPP to reach equilibrium in terms of its photon absorption, scattering, and fluorescence activities.[30] Moreover, the initial TSPP aggregation (in the first few hours) has totally escaped the UV-vis detection, [30] which is in stark contrast to the instantaneous UV-vis response towards TPMN aggregation. Indeed, the first time-dependent UV-

vis extinction spectrum (Figure 3A) was taken within the measurement dead time (~10 seconds) upon the sample preparation.

The rapid disintegration of TPMN aggregates is also in sharp contrast to the slow disassembly of TSPP both triggered by solvent dilution. It took more than 100 days for the TSPP aggregates formed with 10 μM TSPP to reach its constant optical state upon dilution to 1 μM without changing the solution pH.[30] The drastic difference in the assembly and disassembly kinetics between TSPP and TPMN likely stems from their distinct intramolecular interactions. TSPP aggregation is driven predominantly by its strong intermolecular interactions that lead to the formation of tubular J-aggregates.[31,32] Therefore, during the aggregation process TSPP molecules must be adopt an appropriate orientations in order to forming effective *pi-pi* stacking among the constituent molecules. In contrast, the TPMN aggregation is driven primary by the hydrophobic interactions due to the poor solubility in water. In this case, the TPMN molecules are aggregated together regardless of their relative orientation. In other words, TPMN molecules inside their individual aggregates are randomly oriented and the TPMN aggregated are highly amorphous. The rapid disaggregation of the aggregated TPMN is consistent with this randomness hypothesis and it confirms that the intermolecular interaction among TPMN molecules in individual aggregates must be quite weak.

The photon absorption, scattering, and fluorescence intensities of the TPMN aggregates vary as a function of the TPMN disaggregation time (Figure 4). Fruitfully, the time-courses of intensity change can all be empirically fitted by an exponential decay function of $y = A_1 e^{(-kt)}$, allowing quantitatively comparison of effect of the TPMN disaggregation on various optical properties. The decay time-constant k for peak fluorescence intensity (Figure 4J and 4K), light scattering extinction (Figure 4F and 4G), and light scattering depolarization (Figure 4D and 4E) are

approximately two times as those for the TPMN extinction (Figure 4B and 4C) and absorption extinction (Figure 4H and 4I) at the fluorescence excitation wavelength. The faster light scattering reduction is expected before the light scattering cross-section is proportional to the square of the scatterers of volume. Since the ratio between IFE-corrected fluorescence emission intensity and the light absorption extinction is proportional to the fluorescence quantum yield, the data in Figure 4 shows that the fluorescence quantum yield of the AIE aggregates decays as the TPMN aggregates dissolve. The mechanism of such fluorescence quantum yield decay is currently unknown due to the difficulty in experimental probing the TPMN disaggregation pathway, correlation between TPMN size and their optical properties, and the intermolecular interactions among the TPMN molecules in the aggregates and their dependence on the TPMN dissolution. Another imaginable complication is that the optical properties of the outermost molecules in TPMN aggregates most likely are different from that for the inner molecules. Such a surface effect becomes increasingly prominent as the TPMN disaggregation proceeds.

CONCLUSIONS

AIE aggregates are optically complex materials because they are photon absorbers, scatterers, and fluorescence emitters. PRS2 spectroscopic method is effective in separating photon scattering and absorption contribution to UV-vis extinction spectra of the AIE aggregates, allowing quantitative determination of the AIE fluorescence activities obtained with different solvent compositions and AIEgen concentrations. The most critical new findings enabled by the PRS2 method include 1) light scattering extinction can be a significant contributor to the total photon extinction of the TPMN aggregates measured by the UV-vis spectrophotometer. 2) Sample incubation reduces the photon absorption of the TPMN aggregates, but enhances their fluorescence quantum yields. Furthermore, since the enhancement induced by the sample incubation in the

TPMN fluorescence quantum yield is more than enough to compensate the reduction in its photon absorption, the overall fluorescence intensity of the aggregated TPMN is enhanced by the sample incubation. 3) TPMN aggregation is an entirely reversible process, i.e, the aggregated TPMN is readily disintegrated by increasing the fraction of its good solvent. Such disaggregation is empirically a first order process, inducing exponential decay in the TPMN photon absorption, scattering, and emission activities. 4) The rapid aggregation and disaggregation of the aggregated TPMN strongly indicates that TPMN aggregation is driven predominantly due to hydrophobic interactions and the intermolecular interaction within the TPMN aggregates must be very weak. While the generality of these observations to other AIE materials remain to be investigated, the technique presented in this work should be applicable for all AIE materials research. With its ability to provide information important to AIE materials characterization but inaccessible before with existing techniques, the newly developed PRS2 can be a powerful tool for developing quantitative understanding of the structure and property correlation of the AIE materials and for *in-situ* monitoring the AIE aggregation/disaggreation processes.

ASSOCIATED CONTENT

Supporting Information. PRS2 data analysis, DLS data and as-acquired SSF spectra for TPMN water fraction series samples. UV-vis, SSF and PAOS spectra of water series samples. PRS2 data analysis and DLS data for TPMN concentration series samples. As-acquired spectroscopic data for TPMN aggregates as a function of sample incubation. Photographs and as-acquired data for TPMN aggregate disintegration.

AUTHOR INFORMATION

Corresponding Author

*E-mail: Dongmao@chemistry.msstate.edu

Tel: (662) 325-6752

ACKNOWLEDGEMENTS

The authors thank Y. Randika Perera from Dr. Nicholas Fitzkee's group at Mississippi State University for help with the DLS measurements. This work was supported by NSF funds (CHE 1151057) and (EPS-0903787) provided to D.Z. and ACS Division of Analytical Chemistry Summer Graduate Fellowship sponsored by the Society for Analytical Chemists of Pittsburgh provided to J.X.

REFERENCES

(1) Hong, Y.; Lam, J. W. Y.; Tang, B. Z. Aggregation-induced emission, *Chem. Soc. Rev.* **2011**, *40*, 5361-5388.

(2) Wu, W.; Ye, S.; Yu, G.; Liu, Y.; Qin, J.; Li, Z. Novel Functional Conjugative Hyperbranched Polymers with Aggregation-Induced Emission: Synthesis Through One-Pot "A2+B4" Polymerization and Application as Explosive Chemsensors and PLEDs, *Macromol. Rapid Commun.* **2012**, *33*, 164-171.

(3) He, Z.; Ke, C.; Tang, B. Z. Journey of Aggregation-Induced Emission Research, *ACS Omega* **2018**, *3*, 3267-3277.

(4) Deng, H.; Hu, R.; Zhao, E.; Chan, C. Y. K.; Lam, J. W. Y.; Tang, B. Z. One-Pot Three-Component Tandem Polymerization Toward Functional Poly(arylene thiophenylene) with Aggregation-Enhanced Emission Characteristics, *Macromolecules* **2014**, *47*, 4920-4929.

(5) Wang, M.; Yang, N.; Guo, Z.; Gu, K.; Shao, A.; Zhu, W.; Xu, Y.; Wang, J.; Prud'homme, R. K.; Guo, X. Facile Preparation of AIE-Active Fluorescent Nanoparticles through Flash Nanoprecipitation, *Ind. Eng. Chem. Res.* **2015**, *54*, 4683-4688.

(6) Chen, Y.; Lam, J. W. Y.; Kwok, R. T. K.; Liu, B.; Tang, B. Z. Aggregation-induced emission: fundamental understanding and future developments, *Mater. Horiz.* **2019**, *6*, 428-433.

(7) Shao, A.; Xie, Y.; Zhu, S.; Guo, Z.; Zhu, S.; Guo, J.; Shi, P.; James, T. D.; Tian, H.; Zhu, W.-H. Far-Red and Near-IR AIE-Active Fluorescent Organic Nanoprobes with Enhanced Tumor-Targeting Efficacy: Shape-Specific Effects, *Angew. Chem. Int. Ed.* **2015**, *54*, 7275-7280.

(8) Feng, G.; Liu, B. Aggregation-Induced Emission (AIE) Dots: Emerging Theranostic Nanolights, *Acc. Chem. Res.* **2018**, *51*, 1404-1414.

(9) Liu, Y.; Zhao, Z.; Lam, J. W. Y.; Zhao, Y.; Chen, Y.; Liu, Y.; Tang, B. Z. Cascade Polyannulation of Diyne and Benzoylacetonitrile: A New Strategy for Synthesizing Functional Substituted Poly(naphthopyran)s, *Macromolecules* **2015**, *48*, 4241-4249.

(10) Zhu, X.; Liu, R.; Li, Y.; Huang, H.; Wang, Q.; Wang, D.; Zhu, X.; Liu, S.; Zhu, H. An AIE-active boron-difluoride complex: multi-stimuli-responsive fluorescence and application in data security protection, *Chem. Commun.* **2014**, *50*, 12951-12954.

(11) Qiu, Z.; Liu, X.; Lam, J. W. Y.; Tang, B. Z. The Marriage of Aggregation-Induced Emission with Polymer Science, *Macromol. Rapid Commun.* **2019**, *40*, 1800568.

(12) Pao, Y. H.; Mow, C. C. Scattering of Plane Compressional Waves by a Spherical Obstacle, *J. Appl. Phys.* **1963**, *34*, 493-499.

(13) Ooyama, Y.; Sugino, M.; EnoKi, T.; Yamamoto, K.; Tsunoji, N.; Ohshita, J. Aggregation-induced emission (AIE) characteristic of water-soluble tetraphenylethene (TPE) bearing four sulfonate salts, *New J. Chem.* **2017**, *41*, 4747-4749.

(14) Chen, J.; Law, C. C. W.; Lam, J. W. Y.; Dong, Y.; Lo, S. M. F.; Williams, I. D.; Zhu, D.; Tang, B. Z. Synthesis, Light Emission, Nanoaggregation, and Restricted Intramolecular Rotation of 1,1-Substituted 2,3,4,5-Tetraphenylsiloles, *Chem. Mater.* **2003**, *15*, 1535-1546.

(15) Xu, J. X.; Siriwardana, K.; Zhou, Y.; Zou, S.; Zhang, D. Quantification of Gold Nanoparticle Ultraviolet–Visible Extinction, Absorption, and Scattering Cross-Section Spectra and Scattering Depolarization Spectra: The Effects of Nanoparticle Geometry, Solvent Composition, Ligand Functionalization, and Nanoparticle Aggregation, *Analytical Chemistry* **2018**, *90*, 785-793.

(16) Vithanage, B. C. N.; Xu, J. X.; Zhang, D. Optical Properties and Kinetics: New Insights to the Porphyrin Assembly and Disassembly by Polarized Resonance Synchronous Spectroscopy, *The Journal of Physical Chemistry B* **2018**, *122*, 8429-8438.

(17) Athukorale, S. A.; Zhou, Y.; Zou, S.; Zhang, D. Determining the Liquid Light Scattering Cross Section and Depolarization Spectra Using Polarized Resonance Synchronous Spectroscopy, *Analytical Chemistry* **2017**, *89*, 12705-12712.

(18) Xu, J. X.; Vithanage, B. C. N.; Athukorale, S. A.; Zhang, D. Scattering and absorption differ drastically in their inner filter effects on fluorescence, resonance synchronous, and polarized resonance synchronous spectroscopic measurements, *Analyst* **2018**, *143*, 3382-3389.

(19) Xu, J. X.; Liu, M.; Athukorale, S.; Zou, S.; Zhang, D. Linear Extrapolation of the Analyte-Specific Light Scattering and Fluorescence Depolarization in Turbid Samples, *ACS Omega* **2019**, *4*, 4739-4747.

(20) Lakowicz, J. R. *Principles of fluorescence spectroscopy*; New York : Springer, [2006]

3rd ed., 2006.

(21) Leung, N. L. C.; Xie, N.; Yuan, W.; Liu, Y.; Wu, Q.; Peng, Q.; Miao, Q.; Lam, J. W. Y.; Tang, B. Z. Restriction of Intramolecular Motions: The General Mechanism behind Aggregation-Induced Emission, *Chem.: Eur. J.* **2014**, *20*, 15349-15353.

(22) Fu, W.; Yan, C.; Guo, Z.; Zhang, J.; Zhang, H.; Tian, H.; Zhu, W.-H. Rational Design of Near-Infrared Aggregation-Induced-Emission-Active Probes: In Situ Mapping of Amyloid-β Plaques with Ultrasensitivity and High-Fidelity, *J. Am. Chem. Soc.* **2019**, *141*, 3171-3177.

(23) Hong, Y.; Lam, J. W. Y.; Tang, B. Z. Aggregation-induced emission: phenomenon, mechanism and applications, *Chem. Commun.* **2009**, 4332-4353.

(24) Siriwardana, K.; Vithanage, B. C. N.; Zou, S.; Zhang, D. Quantification of the Depolarization and Anisotropy of Fluorophore Stokes-Shifted Fluorescence, On-Resonance Fluorescence, and Rayleigh Scattering, *Anal. Chem.* **2017**, *89*, 6686-6694.

(25) Siriwardana, K.; Vithanage, B. C. N.; Zou, S.; Zhang, D. Quantification of the Depolarization and Anisotropy of Fluorophore Stokes-Shifted Fluorescence, On-Resonance Fluorescence, and Rayleigh Scattering, *Analytical Chemistry* **2017**, *89*, 6686-6694.

(26) Xu, J. X.; Yuan, Y.; Zou, S.; Chen, O.; Zhang, D. A Divide-and-Conquer Strategy for Quantification of Light Absorption, Scattering, and Emission Properties of Fluorescent Nanomaterials in Solutions, *Anal. Chem.* **2019**.

(27) Wang, D.; Su, H.; Kwok, R. T. K.; Shan, G.; Leung, A. C. S.; Lee, M. M. S.; Sung, H. H. Y.; Williams, I. D.; Lam, J. W. Y.; Tang, B. Z. Facile Synthesis of Red/NIR AIE Luminogens with Simple Structures, Bright Emissions, and High Photostabilities, and Their Applications for Specific Imaging of Lipid Droplets and Image-Guided Photodynamic Therapy, *Adv. Funct. Mater.* **2017**, *27*.

(28) Nettles, C. B.; Hu, J.; Zhang, D. Using Water Raman Intensities To Determine the Effective Excitation and Emission Path Lengths of Fluorophotometers for Correcting Fluorescence Inner Filter Effect, *Anal. Chem.* **2015**, *87*, 4917-4924.

(29) Xu, J. X.; Vithanage, B. C. N.; Athukorale, S. A.; Zhang, D. Scattering and absorption differ drastically in their inner filter effects on fluorescence, resonance synchronous, and polarized resonance synchronous spectroscopic measurements, *Analyst* **2018**, *143*, 3382-3389.

(30) Vithanage, B. C. N.; Xu, J. X.; Zhang, D. Optical Properties and Kinetics: New Insights to the Porphyrin Assembly and Disassembly by Polarized Resonance Synchronous Spectroscopy, *J. Phys. Chem. B* **2018**, *122*, 8429-8438.

(31) Micali, N.; Mallamace, F.; Romeo, A.; Purrello, R.; Monsù Scolaro, L. Mesoscopic Structure of meso-Tetrakis(4-sulfonatophenyl)porphine J-Aggregates, *J. Phys. Chem. B* **2000**, *104*, 5897-5904.

(32) Kitahama, Y.; Kimura, Y.; Takazawa, K. Study of Internal Structure of meso-Tetrakis (4-Sulfonatophenyl) Porphine J-Aggregates in Solution by Fluorescence Microscope Imaging in a Magnetic Field, *Langmuir* **2006**, *22*, 7600-7604.

TOC

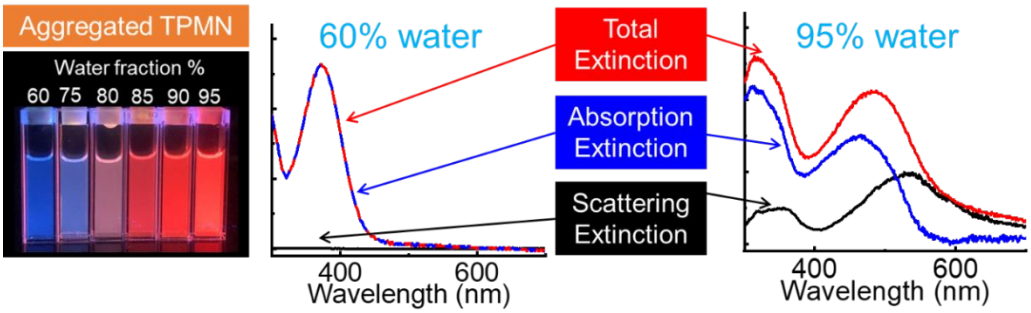
Aggregated TPMN
Water fraction %
60 75 80 85 90 95
60% water
95% water
Total Extinction
Absorption Extinction
Scattering Extinction
400
600
Wavelength (nm)
400
600
Wavelength (nm)